Journal Name

COMMUNICATION

Solid phase polymerization of phenylenediamine toward self-supported FeN_x/C catalyst with high oxygen reduction activity

Received 00th January 20xx,
Accepted 00th January 20xx

DOI: 10.1039/x0xx00000x

www.rsc.org/

Xiaogang Su,[a] Jianguo Liu,[*ab] Yingfang Yao,[ab] Yong You,[a] Xiang Zhang,[a] Canyun Zhao,[a] Hong Wan,[a] You Zhou,[a] and Zhigang Zou[*ab]

Solid phase polymerization of phenylenediamine with template toward self-supported FeN_x/C catalyst was introduced. Using ZnO nanoparticles as hard template could increase the surface area of catalyst, thus the oxygen reduction activity was radically enhanced, to 21.9 Ag^{-1} at 0.80 V (vs.RHE) in acid medium.

Proton exchange membrane fuel cell (PEMFC) is an environment-friendly power supply, which could be the substitution for internal-combustion engine and reduce carbon emissions.[1] However, the large-scale application of PEMFC is severely hindered by high prices, and the high cost is primarily due to platinum catalyst used in the cathode.[2] Recently, non-precious metal catalysts for cathodic oxygen reduction reduction (ORR) have attracted great research interests as alternatives to platinum-based materials.[3] The FeN_x/C catalyst, which is a typical non-precious metal catalyst, is the most likeliest candidate because it exhibits excellent ORR activity in acid medium.[4] Usually, the FeN_x/C catalyst is synthesized by heating the mixture of nitrogen-containing precursors, carbon black, and iron salts.[5] And aniline derivatives are constantly used as the nitrogen source of FeN_x/C catalyst, because of the favorable structure of aromatic rings connected via imino group, which could promote the incorporation of nitrogen-containing active sites into the graphitized carbon framework.[6] For example, Zelenay et al. synthesized a high-performance FeN_x/C catalyst by the directly polymerization of aniline in water. The ORR activity of polyaniline-based FeN_x/C catalyst is ~6.7 Ag^{-1} at 0.80 V (versus reversible hydrogen electrode, vs.RHE).[7] Later, Sun et al. used phenylenediamine as nitrogen source, and prepared a poly-m-phenylenediamine-based FeN_x/C catalyst by aqueous polymerization. And its ORR activity is better, reaching 11.5 Ag^{-1} at 0.80 V.[8] However, the polymerization of aniline derivatives in water is very complex,[9] the preparation process is rather time-consuming and the aqueous polymerization of aniline derivatives can contaminate water. Meanwhile, the morphology of products are affected by polymerization process, pH value, temperature, and so on,[10] which have a great effect on the catalytic activity of FeN_x/C catalyst. What's more, one major problem of FeN_x/C catalysts is the low density of active sites. In single cell test, the loading of FeN_x/C catalyst is much higher than Pt/C catalyst, which leads to the increase of internal resistance and the resistance of mass transfer.[11] In the course of aqueous polymerization, carbon black is needed, which can improve the dispersing performance of products. However, the catalytic activity of carbon black for oxygen reduction is very low, which may lower the density of active sites.

In 2009, Dodelet et al. reported that the greatest increase in active sites density was obtained when a mixture of solid precursors was ball-milled and then pyrolyzed twice.[11] Latter, they found that the exchange of metal ions between ZIF-8 and the Fe complex has detrimental effect on the fuel-cell performance of Fe-based catalysts, and the catalyst prepared by directly ball milling the precursors showed better ORR activity.[12] Therefore, the grinding method to mix solid precursors is a facile and efficient way to prepare Fe-based catalysts, and it can be applied to the polymerization of aniline derivatives, too. Phenylenediamine, ammonium persulfate and ferric chloride hexahydrate are all solid, we just need to grind them together, then raise the temperature to accelerate the polymerisation rate. Besides, the final self-supported FeN_x/C catalyst without adding carbon black can increase the density of active sites and improve the ORR activity. Herein, we report the solid phase polymerization of phenylenediamine with ZnO nanoparticle template toward self-supported FeN_x/C catalyst, the oxygen reduction activity of which is rather high, reaching 21.9 Ag^{-1} at 0.80 V (vs.RHE).

The self-supported FeN_x/C catalyst was prepared through pyrolysis of the mixture of poly-p-phenylenediamine (PpPD) and $FeCl_3$, and PpPD was synthesized by solid phase polymerization. In brief, p-phenylenediamine, zinc oxide nanoparticles (99.8% metals basis, 90±10 nm), ammonium persulfate and ferric chloride hexahydrate were ground together, then transferred to hydrothermal synthesis reactor and heated to 150 °C. Zinc oxide nanoparticles were used as hard template to increase the Brunauer–Emmett–Teller (BET) surface area of PpPD, and they could easily be removed in acid-washing process. After solid state polymerization, the

[a] Eco-materials and Renewable Energy Research Center, Department of Materials Science and Engineering, National Laboratory of Solid State Microstructures, Nanjing University, Nanjing China 210093
[b] Kunshan Innovation Institute of Nanjing University, Nanjing China 210093
E-mail: jianguoliu@nju.edu.cn, zgzou@nju.edu.cn

Electronic Supplementary Information (ESI) available: Experimental details and characterization. See DOI: 10.1039/x0xx00000x mixtures were subjected to first pyrolysis, acid-washing, and second pyrolysis according to the literature methods.[7] The temperature of first and second pyrolysis were both 950 °C. The prepared catalyst was named as PpPD-Fe-ZnO. Al_2O_3 nanoparticles (99.99% metals basis, γ phase, 20 nm) were also used as hard template, and the catalyst was named as PpPD-Fe-Al_2O_3. In addition, PpPD-Fe was also prepared as control sample.

Figure 1a shows a typical transmission electron microscope (TEM) image of PpPD-Fe. The PpPD-Fe has a clumpy morphology, and the particle size is at micro-scale. Moreover, metal-containing particles can be easily observed, and they are encapsulated in graphitic carbon framework. N_2 adsorption–desorption tests are carried out to analyze the interfacial pore structures (Figure 1d), and they show that the BET surface area of PpPD-Fe is only 122 m^2g^{-1}. After heat-treatment, Al_2O_3 nanoparticles are difficult to soluble in sulfuric acid, and TEM image of PpPD-Fe-Al_2O_3 shows that Al_2O_3 nanoparticles closely aggregate on the surface of PpPD (Figure 1b).The BET surface area of PpPD-Fe-Al_2O_3 doubles, to 251 m^2g^{-1}, because of the adding of Al_2O_3. Figure 1c reveals that PpPD-Fe-ZnO consists of a three dimensional disordered pore system and a thin shell, which exactly reflects the geometric characteristics of ZnO nanoparticles packing in the PpPD-based composites. What's more, no obvious metal-containing particles are observed, which means the dispersion of iron salt is more uniform. And the BET surface area PpPD-Fe-ZnO is about nine times bigger than PpPD-Fe, to 1216 m^2g^{-1}. The increase of BET surface is mainly from the morphological change of PpPD. As mentioned above, PpPD-Fe has a clumpy morphology, while PpPD-Fe-ZnO presents a thin shell morphology. As a result, the addition of ZnO template changes the morphology of PpPD, thus the BET surface area of PpPD-Fe-ZnO greatly increases. The corresponding pore size distribution plots (Figure 1d inset) indicate the increase of micropore area (515 m^2g^{-1}) and external surface area (700 m^2g^{-1}), and the hierarchical porous structure is formed.

Figure 2a shows the X-ray diffraction (XRD) patterns of the prepared catalysts. For PpPD-Fe and PpPD-Fe-ZnO, two broad peaks centred at 25.3° and 43.7° appear, which indicate the highly-perfect graphitization structure. But for PpPD-Fe-Al_2O_3, graphite characteristic peak is not observed, and the peaks of XRD match well with standard pattern of γ-Al_2O_3 (JCPDS card

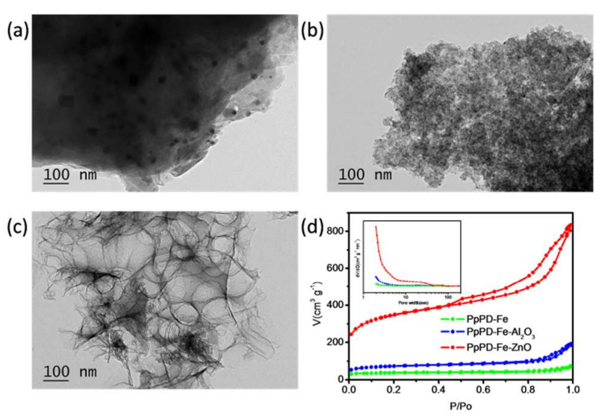

Figure 1. TEM images of (a) PpPD-Fe, (b) PpPD-Fe- Al_2O_3, and (c) PpPD-Fe-ZnO. (d) N_2 adsorption/desorption isotherms and the corresponding pore size distribution (inset) of the above three catalysts.

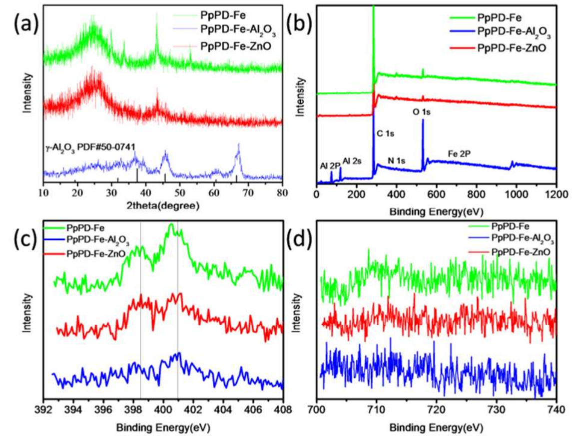

Figure 2. (a) XRD, (b) XPS survey spectrum, (c) high resolution N 1s spectrum, and (d) high resolution Fe 2p spectrum of PpPD-Fe, PpPD-Fe-Al_2O_3, and PpPD-Fe-ZnO.

No: 50-0741), which is consistent with Figure 1b. X-ray photoelectron spectroscopy (XPS) is also carried out to probe the chemical composition and structure of the prepared catalysts. As shown in Figure 2b, the survey spectrum of PpPD-Fe-ZnO reveals the presence of C, N, O, S and less than 0.5 percent (At.%) of Fe and Zn, which is similar to PpPD-Fe. And it reveals that ZnO can be removed completely after acid leaching. But the peaks of Al 2P and Al 2s clearly appear in the survey spectrum of Al_2O_3, and the Al content is found to be 12.5 At.%, which gives a further verification on the residue of Al_2O_3. Nitrogen doped into the carbon structure perform a major role inducing ORR activity of FeN_x/C catalyst, and high resolution N 1s spectrum (Figure 2c) is used to determine the bonding configurations of N atoms. Two dominant types of nitrogen is found in three prepared samples, and they are quaternary-N (401.1 eV) and pyridinic-N (398.5 eV).[13] However, there are no significant differences between three catalysts. And because of the low content of Fe, no obvious peak is observed in Fe 2P spectrum (Figure 2d).

ORR polarization curves of the prepared catalysts are measured on a rotating disc electrode (RDE) in O_2-saturated 0.1M $HClO_4$ solution, with background capacitive current corrected. As shown in Figure 3a, the PpPD-Fe has very low ORR activity. Its current density increases slowly as potential decreases, and the current density at 0 V is only 2.8 $mAcm^{-2}$. As for PpPD-Fe-Al_2O_3, the ORR activity is better, but the improvement is very limited. Surprisingly, the ORR activity of PpPD-Fe-ZnO is radically enhanced, reflected by the appearence of diffusion-limiting current density and the half-wave potential (～0.82 V). The half wave potential of PpPD-Fe-ZnO is only 40 mV lower than that of Pt/C. To quantitatively compare the intrinsic activity, kinetic current density is calculated through Koutecky-Levich equation. Figure 3b shows Tafel plots (Potential vs. Log(j)) of the above catalysts. PpPD-Fe, PpPD-Fe-Al_2O_3 and PpPD-Fe-ZnO have similar Tafel slope, 70, 60, and 60 mV Dev^{-1} respectively. Then kinetic current density is normalized with catalyst loading(0.9 $mgcm^{-2}$) to obtain mass activity (j_m).The measured mass activities of PpPD-Fe, PpPD-Fe-Al_2O_3 and PpPD-Fe-ZnO are 0.272, 0.466 and 21.8

Ag^{-1} at 0.80 V (Figure 3c). Obviously, the ORR activity of PpPD-Fe-ZnO is far

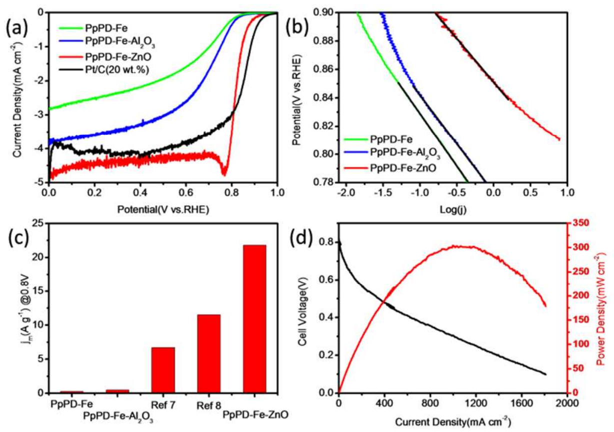

Figure 3. (a) ORR polarization curves of PpPD-Fe, PpPD-Fe-Al_2O_3, PpPD-Fe-ZnO and Pt/C in O_2-saturated 0.1 M $HClO_4$ solution. Rotating speed: 900 rpm; scan rate: 10 mVs^{-1}; FeN_x/C catalyst loading: 0.9 $mgcm^{-2}$. (b) Tafel plots obtained from the RDE measurements. (c) ORR mass activity at 0.80 V of catalysts. (d) Polarization and power density plots for H_2-O_2 single fuel cell with PpPD-Fe-ZnO as cathode catalyst at 80 °C. MEA active area: 0.9 cm^2; Nafion 211 membrane; Cathode catalyst loading: 2.4 $mgcm^{-2}$; Anode catalyst: Pt/C (60 wt%, JM).No back pressure is applied.

better than the other two samples. As mentioned above, there are no significant differences between three samples in XRD and XPS characterization except N_2 adsorption–desorption tests. It is widely believed that micropores host most of the catalytic sites, and large microporous surface area can supply many accessible active sites, while great external surface area is conducive to the efficient mass transport.[14] The BET surface area of PpPD-Fe is only 122 m^2g^{-1}, so its ORR activity is poor. As for PpPD-Fe-Al_2O_3, the BET surface area doubles, therefore, the ORR activity improves limitedly. Thanks to the huge BET surface area and the hierarchical porous structure, the ORR activity of PpPD-Fe-ZnO tremendously improves. Finally, we carry out H_2-O_2 PEMFC test. Membrane electrode assemblies consisted of PpPD-Fe-ZnO as cathode catalyst, and Pt/C as anode catalyst for H_2 oxidation are adopted. In order to reduce the internal resistance of the PEMFC, the loading of cathode catalyst is only 2.4 $mgcm^{-2}$, and no back pressure is applied during the fuel cell test. Figure 3d shows the fuel cell polarization curve and power density plot. The maximal power density can reach to 305 $mWcm^{-2}$ at cell voltage of 0.306 V and current density of 997 $mAcm^{-2}$. In consideration of low loading of cathode catalyst, the cell performance is good, and the mass activitiy of PpPD-Fe-ZnO is rather high.

In conclusion, a green way to prepare FeN_x/C catalyst with high oxygen reduction activity was introduced. The solid phase polymerization of PpPD is facile, and using ZnO as hard template can greatly increase the BET surface area. Besides, the self-supported structure without adding carbon black can increase the mass activity of the FeN_x/C catalyst. Such a solid phase polymerization with template toward FeN_x/C catalyst with high BET surface area opens up new avenues to nanostructured carbon materials for fuel cells, batteries, and supercapacitors.

This work was financially supported by National Science Foundation of China (21176111, 21476104), National Basic Research Program of China (973 Program, 2013CB632404), and Priority Academic Program Development of Jiangsu Higher Education Institutions. Jianguo Liu also thanks to the support of Qing Lan Project of Jiangsu Province, China.

Notes and references

1 J. Tollefson, Nature News, 2010, 464, 1262-1264.
2 R. Borup, J. Meyers, B. Pivovar, Y. S. Kim, R. Mukundan, N. Garland, D. Myers, M. Wilson, F. Garzon and D. Wood, Chemical reviews, 2007, 107, 3904-3951.
3 F. Jaouen, E. Proietti, M. Lefèvre, R. Chenitz, J.-P. Dodelet, G. Wu, H. T. Chung, C. M. Johnston and P. Zelenay, Energy & Environmental Science, 2011, 4, 114-130.
4 H. A. Gasteiger, S. S. Kocha, B. Sompalli and F. T. Wagner, Applied Catalysis B: Environmental, 2005, 56, 9-35.
5 S. Gupta, D. Tryk, I. Bae, W. Aldred and E. Yeager, Journal of applied electrochemistry, 1989, 19, 19-27.
6 S. Bhadra and D. Khastgir, Polymer Degradation and Stability, 2008, 93, 1094-1099.
7 G. Wu, K. L. More, C. M. Johnston and P. Zelenay, Science, 2011, 332, 443-447.
8 Q. Wang, Z.-Y. Zhou, Y.-J. Lai, Y. You, J.-G. Liu, X.-L. Wu, E. Terefe, C. Chen, L. Song and M. Rauf, Journal of the American Chemical Society, 2014, 136, 10882-10885.
9 H. XU, W. YAN and J. FENG, Chemical Industry and Engineering Progress, 2008, 10, 017.
10 W.-S. Huang, B. D. Humphrey and A. G. MacDiarmid, Journal of the Chemical Society, Faraday Transactions 1: Physical Chemistry in Condensed Phases, 1986, 82, 2385-2400.
11 M. Lefèvre, E. Proietti, F. Jaouen and J.-P. Dodelet, science, 2009, 324, 71-74.
12 J. Tian, A. Morozan, M. T. Sougrati, M. Lefèvre, R. Chenitz, J. P. Dodelet, D. Jones and F. Jaouen, Angewandte Chemie, 2013, 125, 7005-7008.
13 G. Wu, M. A. Nelson, N. H. Mack, S. Ma, P. Sekhar, F. H. Garzon and P. Zelenay, Chemical Communications, 2010, 46, 7489-7491.
14 F. Jaouen, M. Lefèvre, J.-P. Dodelet and M. Cai, The Journal of Physical Chemistry B, 2006, 110, 5553-5558.